Check for
updates

Transport of Water Contaminated with Various Ions Through Nanoporous Graphene: A Molecular Dynamics Simulation

Mohammad Rahiminejad[1] · Vahid Mortazavi[1] · Ali Moosavi[1] · Ali Nouri-Borujerdi[1]

Abstract

Through extensive MD simulations, desalination of water contaminated with various ions including Na^+, K^+, Mg^{2+}, Ca^{2+}, and Cl^- through monolayer graphene is explored, and the influences of nanopore diameter, applied pressure, contaminant concentration, and functional groups on the number of permeated water through the membrane and ion rejection are quantified. Obtained results reveal that there exists an optimum pore diameter in which maximum ion rejection by the membrane occurs. Also, it is demonstrated that the hydration energy of ions is potentially effective in ion rejection, so ions with lower hydration energy are more likely to pass through the membrane. This conclusion applies to all contaminant concentrations. Moreover, it is found that the effect of increasing the external pressure on the water permeability is more for the membranes with smaller diameters. This observation may be crucial in designing such membranes. Finally, it is shown that the hydroxylated pore has higher water permeability than the carboxylated pores. In contrast, the carboxylated pore is better at ion rejection than the hydroxylated and pristine pores.

Article Highlights

- The desalination of water contaminated with various ions by graphene is evaluated.
- The effects of pore size, ion concentration, and functional groups are explored.
- The rejection of different ions for nanopores smaller than 9 Å is 100%.
- As ion concentration increases, water permeation through the membrane decreases.
- Water permeation for hydroxylated pore is greater than for carboxylated pore.

✉ Ali Moosavi
moosavi@sharif.edu

[1] Center of Excellence in Energy Conversion (CEEC), School of Mechanical Engineering, Sharif University of Technology, Azadi Avenue, Tehran, Iran

1 Introduction

Water purification is one of the significant challenges of the current world. Drought and freshwater scarcity in a large number of countries around the world have made human access to clean water a substantial and worrying problem. Hence, paying more attention to conserving water resources and developing high-efficiency water treatment technologies is necessary. The great potential of nanotechnology for the removal, control, and treatment of environmental pollution makes it an effective tool for achieving sustainable development in many fields. Advances in nanoscale science and engineering suggest that many of the present problems, such as clean water shortage, can be dramatically eliminated or reduced by nanoadsorbents, nanocatalysis, bioactive nanoparticles, nanopowders, and carbon-based nanomaterial, to name just a few (Wang et al. 2013; Madima et al. 2020; Mudhoo and Sillanpää 2021; Failed 2019). Due to the inherent advantages of membrane processes such as integration, operation without chemical processes, high process intensity, and taking control over them (Teow and Mohammad 2019), the application of nanotechnology in membrane-based desalination processes such as electrodialysis (Campione et al. 2020), ion exchange (Gao et al. 2015), reverse osmosis (RO) (Zhang et al. 2018), forward osmosis (Liu et al. 2018a), and micro-filtration (Chen et al. 2016) has been of high interest in recent years.

Among the various water desalination methods, reverse osmosis is one of the most efficient and common methods. However, the permeation rate of water is very slow in classical reverse osmosis membranes (Cohen-Tanugi and Grossman 2012). Advances in nanotechnology in recent years have made it possible to use high-permeability nano-material. Some of these materials, such as carbon honeycomb (CHC) (Qin et al. 2021), graphyne (Xue et al. 2013), carbon nanotube (CNT) (Lv et al. 2019), graphitic carbon nitride (gCN) (Liu et al. 2018b), molybdenum disulfide (MoS2) (Köhler et al. 2018), boron nitride (Loh 2019), zeolites (Hou et al. 2021), organic–inorganic hybrid porous materials (Chen et al. 2021), and MXene (Meidani et al. 2021), have been tested for desalination. In this regard, graphene, a new class of nanomaterial, is cost-effective and has many exciting properties (Geim and Novoselov 2007). In particular, the quantum properties of graphene-based nanomaterial offer great potential for application in desalination systems (Zhao et al. 2021). Because the water flux of a membrane scales inversely with its thickness (Cohen-Tanugi and Grossman 2012), a thin graphene sheet can be used for the flux increment. Compared to the classical reverse osmosis membranes, two important advantages of this material are high mechanical strength and low-pressure requirement, which eventuate to low cost and energy requirement (Cohen-Tanugi and Grossman 2012). Although many studies have examined the high potential of graphene in fields such as DNA sequencing (Heerema and Dekker 2016), electrodes for environmental sensing (Yang et al. 2019), and photocatalytic materials (Qureshi et al. 2019), the application of this fantastic nanomaterial in membrane-based desalination systems has attracted further attention. Different mechanisms were proposed for graphene manufacturing. Graphene membrane (mainly a single layer) on a substrate of copper was fabricated by Bae et al. (2010) with the chemical vapor deposition method. O'Hern et al. (2014) introduced the permeable pores with controlled dimensions into the single-layer graphene by ion bombardment associated with oxidative etching. Properties and different methods of making porous graphene were reported by Russo et al. (2013). It was shown that single- or few-layer graphene on a large scale could be produced using the chemical vapor deposition method (Kim et al. 2009; Reina et al. 2009;

Cao et al. 2010). The atomic structure of the pores in graphene was studied using an electron microscope with very high accuracy by Robertson et al. (2015). Recently, Huang et al. (2015) provided a comprehensive overview of the various methods of making nanoporous graphene.

The performance of monolayer graphene as a membrane in the RO water treatment system depends on various factors, including pressure gradient, pore size, and contaminant concentration. Also, many studies mentioned that functionalizing the nanopores, charging the membrane, and exerting an electric field with appropriate intensity and direction can enhance the desalination performance of the graphene (Mortazavi et al. 2020; Kamal Kandezi et al. 2020; Nguyen and Beskok 2019, 2020; Rikhtehgaran and Lohrasebi 2015). Cohen-Tanugi and Grossman (2012) demonstrated that functionalized pores in monolayer graphene remarkably impact the separation of sodium chloride from water. Furthermore, they showed that this structure could have a water flow rate several times higher than conventional RO membranes. In another study, they investigated the effect of real pressure used in the reverse osmosis process for water purification across nanoporous graphene membranes (Cohen-Tanugi and Grossman 2014). This result revealed that the graphene membrane retains its high permeability properties even under low pressures. Suk and Aluru (2010) found that a graphene membrane with a pore diameter greater than 0.8 nm can be recommended ahead of a CNT with a similar pore diameter as the first choice for the filtration process. With the help of a similar method, Jun et al. (2011) showed that single-layer graphene can withstand a pressure of 500 MPa. Liu and Chen (2014) studied the mechanical properties and strength of nanoporous graphene and found that increasing the nanopore's size and porosity decreases the graphene's strength. The passage of water molecules, sodium, and chloride ions across a pristine and functionalized porous graphene has been investigated by Konatham et al. (2013). Their results indicated that the small pores grafted with hydroxyl groups, even in solutions with high concentrations, are effective in rejecting chloride ions. The comparison between sodium and potassium permeation through nanopores was made by Liu et al. (2008). According to the reported results, sodium ions have higher rejection rates due to the higher stability of sodium–water clusters compared to potassium–water. In a study conducted by Sint et al. (2008), the performance of monolayer graphene with functionalized nanopore was investigated, and it was concluded that fluorine–nitrogen-terminated nanopore blocks the permeation of anions, while hydrogen-terminated nanopore rejects the cations. Wang et al. (2017) examined water treatment through nanoporous graphene membranes functionalized with hydrogen or hydroxyl groups. They obtained that the water flux through the membrane scales linearly with applied pressure and nanopore diameter. Chogani et al. (2020) revealed that the proper distribution of alkyl chemical groups in nanopores could lead to the complete rejection of the ions from permeating across the single-layer graphene membrane. Also, they found that the membrane performance in terms of ion repulsion and water flux decreased with the rising concentration of salt.

As reported above, graphene membranes have numerous advantages in water purification systems. Therefore, applying these structures in removing pollutants from industrial wastewater and desalinating saline water of the seas and oceans can undoubtedly save energy and the environment. Although there are many investigations on water transport across a monolayer graphene membrane, the effects of various ions simultaneously dissolved in water are rarely considered. In contrast, saline water sources in the seas, lakes, and oceans contain large amounts of various pollutants such as sodium, calcium, potassium, and magnesium. So, in the present study, water filtration with different contaminant ions (i.e., sodium, calcium, potassium, magnesium, and chlorine) through a single-layer

graphene membrane is investigated. Also, the influences of nanopores diameter, external pressure, contaminant concentration, and functional groups grafted into pores on water flux and ion rejection across the monolayer graphene membrane are quantified.

2 The Method

Molecular dynamics (MD) simulations were conducted to study water desalination by a single-layer graphene membrane. Figure 1 indicates the simulation box used in the present study. As can be seen, the simulation box consists of three parts: the saline water reservoir, the clean water reservoir, and the single-layer graphene membrane. The saline water reservoir (left box) initially contained 1537 water molecules contaminated with different concentrations of pollutant ions (0.1, 0.2, and 0.3 mol/L). All the pollutant salts (NaCl, KCl, $MgCl_2$, and $CaCl_2$) were considered simultaneously by adding an appropriate number of each ion (Na^+, K^+, Mg^{2+}, Ca^{2+}, and Cl^-) to the left box so that the system is charge neutral. The number of ions for each case is listed in Table S1. These ions were randomly distributed in the feed box and could move freely. The clean water reservoir (right box) was initially filled with 546 water molecules. It was separated from the left box by the graphene membrane with 416 carbon atoms and dimensions of 30×30 Å^2 placed in $z=0$ (parallel to the xy-plane). As mentioned before, it was reported that monolayer graphene with a pore diameter higher than 8 Å is more reasonable than a CNT with the same diameter for water permeability (Suk and Aluru 2010). Therefore, different nanopores with diameters of 9, 11, 13, and 15 Å were created in the center of the membrane by removing 24, 34, 50, and 68 carbon atoms, respectively (as shown in Fig. 2). Two rigid graphene sheets were located in the $z=-75$ Å and $z=45$ Å to create a pressure gradient in the system. External pressure $P_{ext} = 100$, 150, and 200 MPa and atmospheric pressure were exerted to the left and right pistons, respectively, by applying a constant force $F = (P \times A)/n$ to all carbon atoms of the sheets, where n denotes the number of carbons in each piston and A is the area of the piston. Compared to the pressures used in real RO systems, these high pressures are
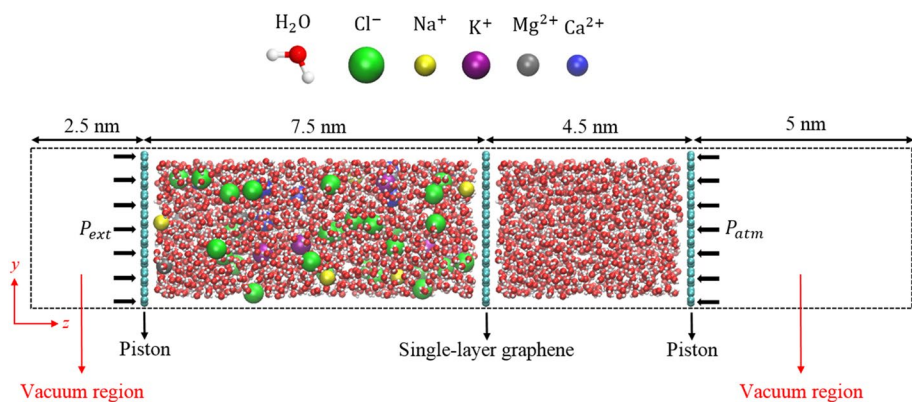
Fig. 1 Schematic representation of the simulated system at the beginning of the simulation containing the saline water box (left) and clean water box (right) separated by the graphene membrane. O, H, C, Cl^-, Na^+, K^+, Mg^{2+}, and Ca^{2+} are colored with red, white, cyan, green, yellow, purple, gray, and blue, respectively. Two vacuum regions are considered outside the pistons to avoid interactions through periodic boundary conditions
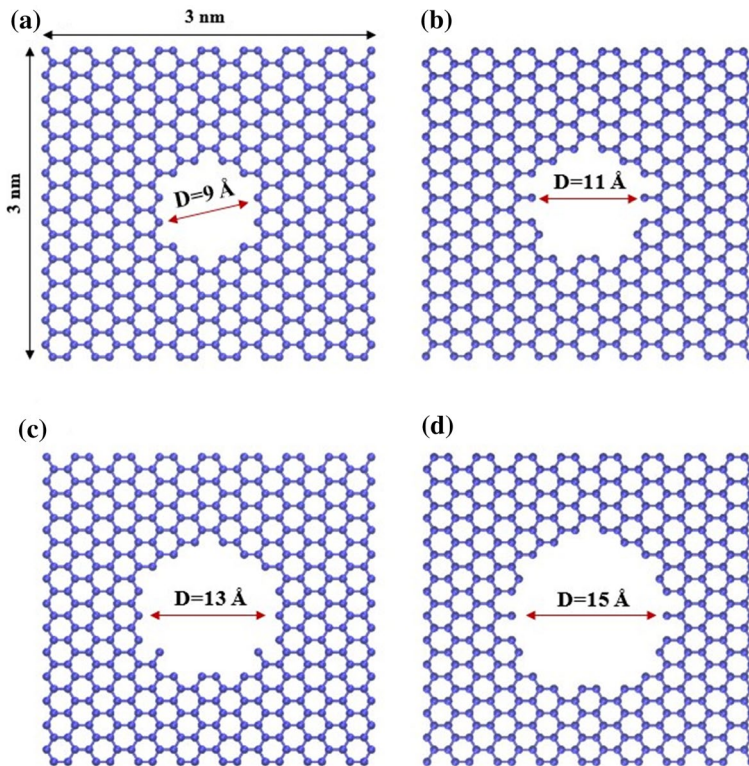
Fig. 2 Graphene membrane with dimensions of 30×30 Å^2 and different pore diameters. The pore diameters for the cases **a**, **b**, **c**, and **d** are equal to 9, 11, 13, and 15 Å, respectively

considered to decrease the computational cost and speed up the MD simulation (Cohen-Tanugi and Grossman 2012; Liu et al. 2016).

In addition, to evaluate the effects of functional groups on the desalination performance of the membrane, equal numbers of hydroxyl (OH) and carboxyl (COO⁻) groups were grafted into the carbon at the pore edge (Fig. 3). The OPLS-AA force field parameters (Konatham et al. 2013; Jorgensen et al. 1996) were used to model functional groups, whose details were summarized in Table S2, Table S3, and Table S4. Water molecules were modeled using the four-site TIP4P potential (Cohen-Tanugi and Grossman 2012; Jorgensen et al. 1983), as this model is an appropriate choice for reproducing water's entropy and hydrogen bonds with high accuracy (Zielkiewicz 2005). SHAKE algorithm was employed to fix the O–H bond and the H–O–H angle of water molecules at values of 0.9572 Å and 104.52°, respectively. The AIREBO potential was used for the carbon atoms interactions in the graphene membrane. Solvated ions were modeled with suggested potentials from previous studies (Joung and Cheatham 2008; Chen and Yang 2015; Dang 1995). The Lennard-Jones parameters and charge of all species are summarized in Table S5. Also, LJ interactions between unlike atoms were modeled using the Lorentz−Berthelot mixing rules (Kong 1973). The cutoff radius for electrostatic and van der Waals interactions was 10 Å and 12 Å, respectively. Long-range electrostatic interactions were treated using the parti-cle–particle–particle–mesh (PPPM) solver (Hockney and Eastwood 1988), and the periodic
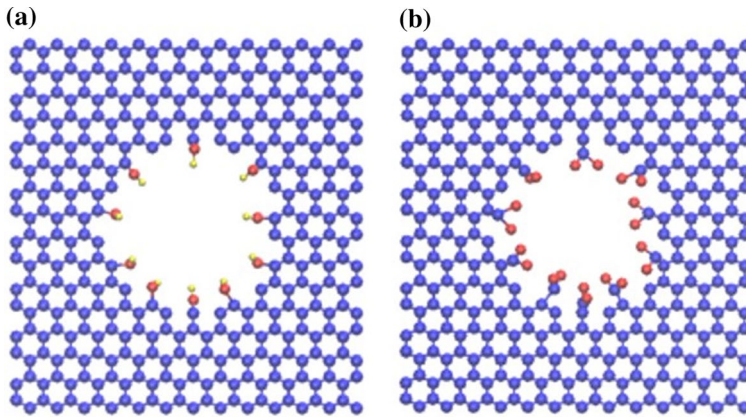
Fig. 3 Schematic of the functionalized pores. **a** Hydroxylated pore, **b** carboxylated pore

boundary conditions were exerted in all directions. All simulations were performed using the LAMMPS MD program (Plimpton 1995).

Gaussian velocity distribution consistent with 300 K was used for the initial velocity of the particles. In the first part of the simulation, the system was equilibrated under NVT ensemble at 300 K for 50 ps. At the same time, the external pressures on the pistons were kept at 1 atm to bring the water density in each reservoir to about 1 g/cm^3. In the second step, the nanopore was created in the center of the graphene, and the simulation was carried out in the NVT ensemble. At the same time, the desired external pressure was applied to the left piston to establish the water flow in the system. All simulations were performed for 5–15 ns with the time step of 1 fs, and the equations of motion were solved by the velocity Verlet method. The properties reported in the following were calculated by averaging over three separate simulations to have reliable results.

3 Results and Discussion

3.1 Effect of the Pore Diameter

As mentioned previously, four nanopores with diameters 9, 11, 13, and 15 Å have been considered to investigate the influences of the pore diameter on the pristine graphene membrane function. Figure 4 shows the number of filtered water molecules across the nanopores over time at a pressure of 100 MPa. The slopes of these graphs give the water flow rate, and as expected, increasing the nanopore diameter enhances the flow rate. For instance, after 5 nanoseconds, by increasing the size of the nanopore from 9 to 15 Å, the filtered water will rise about 168%.

It should be noted that osmotic pressure is created within the system due to the concentration difference between the two reservoirs, leading to water molecules' transport from the right reservoir to the left one. This pressure is calculated using the Morse equation $\Delta\Pi = iMRT$, where Π, i, M, R, and T are the osmotic pressure, Van't Hoff factor, molar concentration (in mol/L), the universal gas constant, and temperature, respectively (Cohen-Tanugi and Grossman 2014). Considering that the simulation is performed at the

Fig. 4 Number of filtered water molecules across different pristine nanopores with diameters of 9, 11, 13, and 15 Å at the 100 MPa pressure
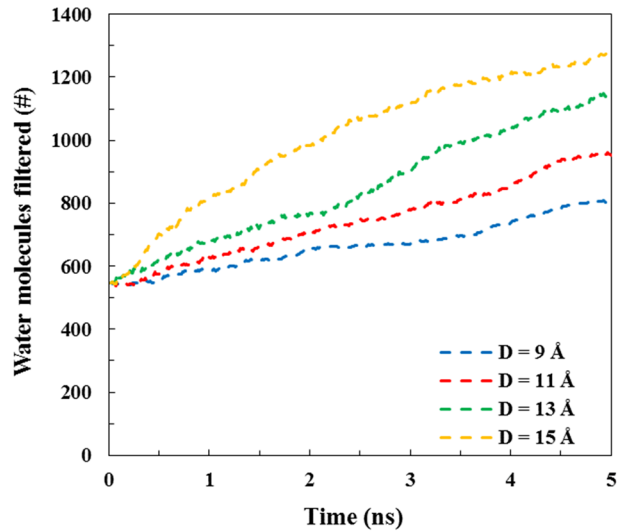
temperature of 300 K and the concentration is 0.2 mol/L, the osmotic pressure difference at the beginning of the simulation will be about 10 bar, which is negligible compared to the external pressure on the left piston. However, as the piston moves and the feed reservoir concentration increases, the osmotic pressure increases and slightly decreases the water molecules' passage through the membrane, which means the water flow rate reduction, as shown in Fig. 4, especially for a diameter of 15 Å.

To further investigate the structure of water, the density profile of water molecules (averaged across *xy*-plane) for the pore diameter of 15 Å (as samples) is plotted in Fig. 5. As can be seen, the density of water is not uniform in all regions of the investigated system. Due to non-bonded interactions between water molecules and the graphene membrane, water molecules accumulate on both sides of the graphene (about ± 4 Å around it), and the intensity of the profile is higher in these regions compared to the bulk. Two peaks near the graphene sheet indicate this phenomenon. The
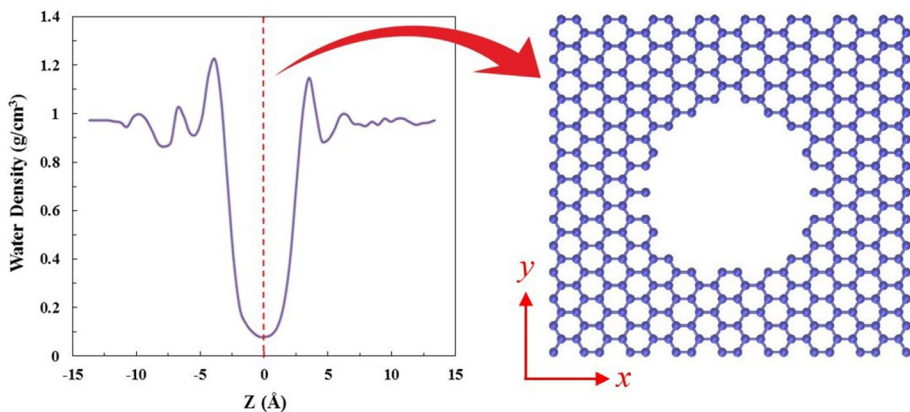
Fig. 5 Density profile of water molecules for pristine graphene membrane with 15 Å pore diameter. The dashed line shows the position of the graphene sheet

water density far from the sheet is 1 g/cm^3, while a layered structure of water is formed in the region adjacent to the sheet. Moreover, Fig. 6 shows the radial distribution functions (RDF) of oxygen–oxygen and hydrogen–hydrogen atoms within the region of 4 Å around the purification membrane and the whole system. As mentioned, the probability of the presence of water molecules in the region of 4 Å near the graphene is more than the whole system, which leads to the greater peak values for RDF of O–O and RDF of H–H. Also, the accumulation of more water molecules causes RDFs to be more fluctuating in this region than in the whole system. Some other researchers have mentioned the same result and concluded that the non-bonded interaction of the oxygen and carbon of the membrane is responsible for the layered structure of water in this region (Azamat et al. 2015). The graphene membrane can be considered as a filter for the water molecules; thus, non-bonded interactions between the atoms cause a tendency for water molecules to accumulate at a specified distance from the graphene.

Also, ion rejection was described as the ratio of remaining ions in the saline water reservoir to the initial ones at the time that half of the water passes through the nanopore (Cohen-Tanugi and Grossman 2012). Figure 7 shows the rejection of various ions examined in this study at a pressure of 100 MPa. According to the results, the pores with diameters smaller than 15 Å block entirely different types of ions, while increasing the nanopore diameter to 15 Å reduces the membrane's ability to excrete potassium and chloride ions. For further investigation, ion rejection for different pore diameters at the pressure of 200 MPa is also plotted in Fig. 8. According to the results, ion rejection for the 9 Å pore diameter is 100% for all ions. Another consequence is that only potassium passes through the 11 Å pore at the pressure of 200 MPa, while the membrane entirely repels the other ion species. By increasing the pore diameter to 13 Å, in addition to potassium ions, a few chloride ions have the opportunity to pass through the membrane. Also, ion rejection for the pore diameter of 15 Å is less than the other pores, which was an expected result. Besides, it can be concluded that increasing the pore diameter is an effective method to enhance the membrane performance in terms of the transport of water molecules; however, it leads to a reduction in ion rejection. Therefore, increasing the pore size has the opposite effect on water flux and ion rejection. For this reason, it alone does not have a favorable impact on membrane efficiency.
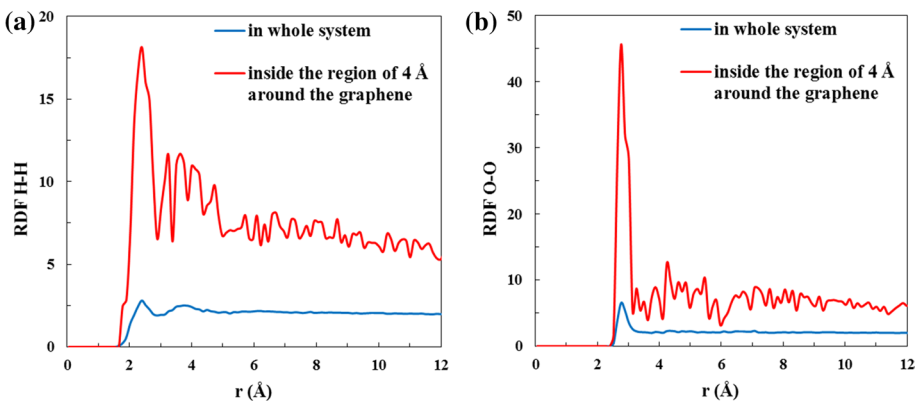

Fig. 6 Radial distribution functions of oxygen–oxygen (**a**) and hydrogen–hydrogen (**b**) atoms in the region of 4 Å around the purification membrane (red line) and in the whole system (blue line)

Fig. 7 Ion rejection of the pristine graphene membrane with different nanopore diameters of 9, 11, 13, and 15 Å at the 100 MPa pressure. The values were computed by averaging over three individual simulations
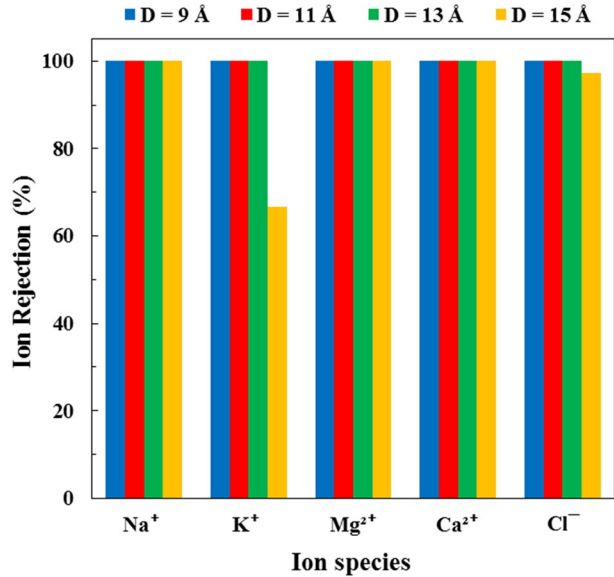
Fig. 8 Ion rejection of the pristine graphene membrane with different nanopore diameters of 9, 11, 13, and 15 Å at the 200 MPa pressure. The values were computed by averaging over three individual simulations
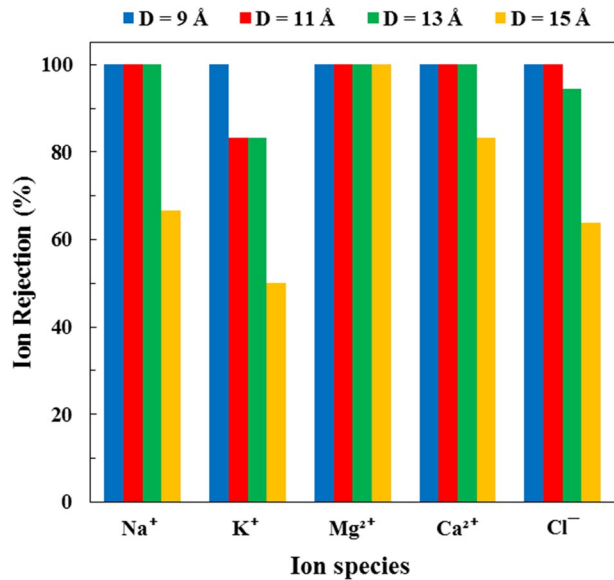
Ionic radius and hydration radius are influential factors in the rejection of ions by the membrane. In an aqueous solution, a shell of water molecules surrounds the ions, called hydration. In this condition, the radius of the hydrated ion (also hydration radius) is larger than the ionic radius, and its comparison with the pore size of the membrane is an influential factor in the mechanism of ion rejection by the membrane. For instance, the ionic radius of Cl^- is equal to 1.84 Å (Table 1), and its hydrated radius is equal to 3.23 Å (Bounds 1985). With the equilibrium vdW distance of $\sigma_{C-O} = 3.282$ Å between

Table 1 Ionic radius and hydration energy values for ions investigated in this study (Wells 1984; Cotton et al. 1999)

| Property	Ion				
	Na^+	K^+	Mg^{2+}	Ca^{2+}	Cl^-
Ionic radius (Å)	1.02	1.38	0.72	1	1.84
Hydration energy (KJ/mol)	− 406	− 322	− 1921	− 1577	− 363

the oxygen atom of the water molecule in the hydration layer and the carbon atom at the edge of the cavity, Cl^- ions can easily pass through the nanopores with diameters of 13 and 15 Å. On the other hand, for Cl^- ions to permeate through the pores with diameters of 9 and 11 Å, it is necessary to remove some water molecules from the hydration shell, for which more energy must be supplied. It can be a plausible reason for weakening the membrane's performance in repelling ions by increasing the size of the nanopores.

Tansel et al. (2009) reported that the sizes of the ions could not be the sole factor for their permeability in the membrane. In this regard, they revealed that the hydration energy, defined as the amount of energy released during the dissolution of one mole of ions, is a more compelling factor to justify this phenomenon. The hydration of each ion is related to its electrostatic adsorption of water molecules. Since the water molecules' adsorption around an ion is related to its charge density, smaller ions, which have more ionic potential (the ratio of electric charge to the ion radius), attract more water molecules. Therefore, the hydration radius is inversely related to the ionic radius (Dove and Nix 1997), and separating water molecules from the hydration structure around smaller ions requires more energy (Havel and Högfeldt 1995). The hydration energy values for the ions investigated in this study are taken from previous works and are summarized in Table 1 (Wells 1984; Cotton et al. 1999). According to the table, by increasing the ionic radius, the hydration energy decreases, and this, in turn, reduces the size of the hydrated ion. Therefore, the possibility of passing the ions through the membrane with low hydration energy will be greater than the others. In addition, by comparing Table 1 with Figs. 7 and 8, it can be concluded that ions with lower hydration energy have more chances to go through the membrane in each pore diameter. In this regard, magnesium's hydration energy (absolute value) is more than the other ions; therefore, this ion has less probability of passing through the membrane. On the other hand, the hydration energy of potassium is lower than the other ions, and as the diameter of the nanopore increases, this ion is more likely to cross the membrane. Liu et al. (2008) also reported similar results for potassium and sodium ions passing through carbon nanotubes.

On the other hand, two ions with a smaller ionic radius (magnesium and calcium) have more considerable hydration energy (absolute value) than the ions with a larger ionic radius (sodium and potassium). Consequently, the larger ions (sodium and potassium) can easily separate from their hydration layers and pass through the membrane (Tansel et al. 2006). In contrast, ions with a larger hydration radius (magnesium and calcium) just in high pressure will have the opportunity to go to the other side of the membrane (Tansel 2012). This inference remains valid for comparing sodium–potassium and magnesium–calcium ions. Another important point that should be mentioned is that the state transition from weak to strong hydration shell is done within a larger radius in monovalent anions compared to monovalent cations. As a result, anions keep their hydration shells stronger than cations with the same charge density (Cotton et al. 1999; Tansel et al. 2006). That is why, despite the same hydration energy of sodium,

potassium, and chloride ions, the average rejection of chloride ions is more than the others.

The radial distribution functions of oxygen atoms around different ions in the bulk region and at a distance of 1 Å from the nanopore center (position of (− 1,0,0)) are represented in Fig. 9 to prove the effect of hydration energy on the ion rejection by the membrane. As an example for Na–O RDF and K–O RDF, because potassium's ionic radius is greater than sodium's (and thus its ionic potential, hydration energy, and hydration radius are smaller), the RDF peak position for K–O will occur at a larger radius compared to Na–O, although the value will be smaller. As a matter of fact, due to the higher ionic
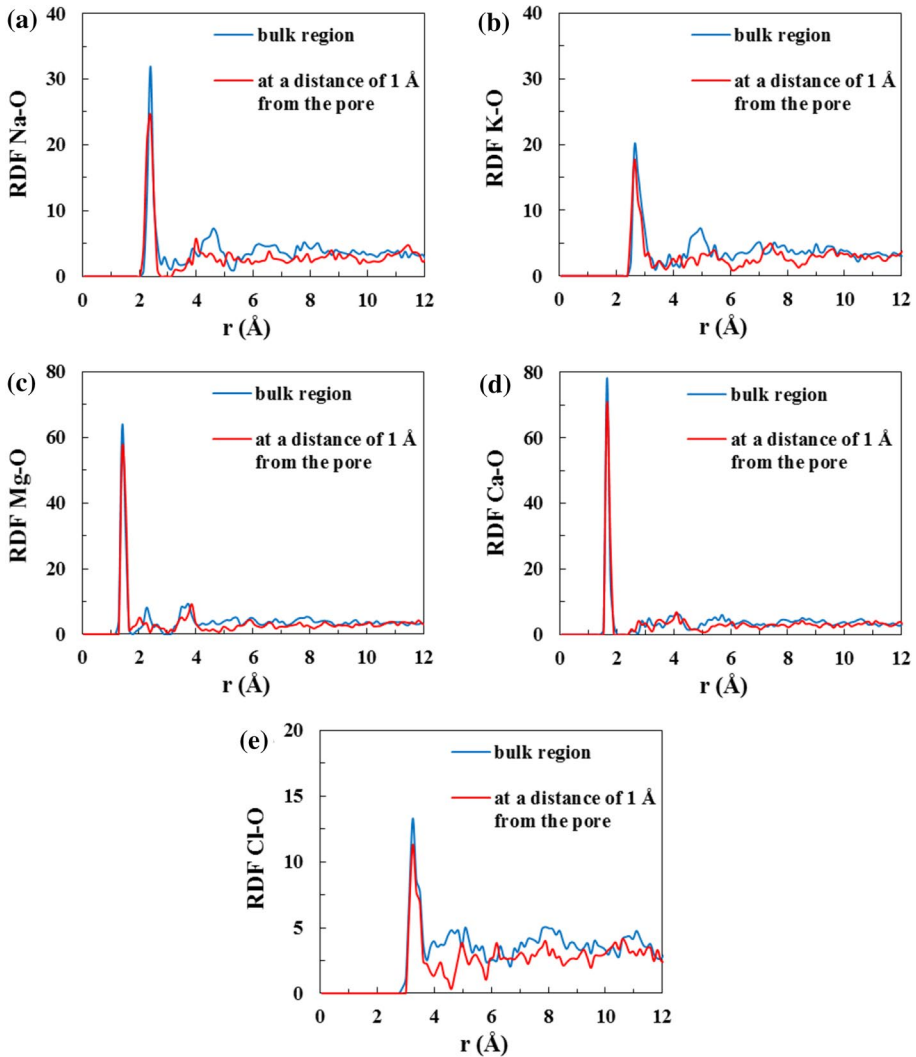
Fig. 9 Radial distribution functions for oxygen atoms around sodium (**a**), potassium (**b**), magnesium (**c**), calcium (**d**), and chlorine (**e**) ions in the bulk region (blue line) and at a distance of 1 Å from the center of the 9 Å nanopore

potential of sodium, it attracts water molecules in its first hydration shell stronger than potassium with a lower ionic potential. (As can be seen in Fig. 9, the intensity of sodium is higher, while the position is smaller.) However, since sodium attracts more water molecules with more required detaching energy, the whole hydrated radius of sodium will be larger than potassium. Therefore, it cannot pass through the membrane as possible as the potassium and has more rejection. Additionally, although it seems that the first hydration shell of the potassium occurs at a larger diameter, sodium has more peaks in its corresponding curve. Consequently, the hydrated radius of sodium will be larger, and it remains neighboring water molecules with more energy (i.e., the solvation shell of sodium is relatively stable). These results are consistent with previous findings (Marañón Di Leo and Marañón 2004; Lee and Rasaiah 1996; Azamat et al. 2014; Impey et al. 1983; Degrève et al. 1274).

Moreover, the hydration number, defined as the number of water molecules in the hydration shell around the ion, can be calculated by integrating the RDF profile from $r = 0$ to the distance where the first minimum of the profile occurred. Hence, the hydration numbers of the ions in the bulk region and position of $(-1,0,0)$ were computed and are summarized in Table 2. The difference between values indicated the number of water molecules that must be detached from the hydration shell for the ion to locate at the pore's entrance and pass through it. Since the separation of water molecules from the hydration shell takes place with energy consumption, the smaller the difference in the hydration number in the two regions, the less energy is needed for the ion to pass through the pore, and as a result, the percentage of ion rejection will be lower. According to Table 2, the potassium's hydration number changes are lower than other monovalent ions, meaning that less energy is required for potassium ions to permeate through the membrane than sodium and chloride ions. Thus, potassium has the lowest rejection percentage among monovalent ions, a result that is consistent with Figs. 7, 8, and Table 1. Also, it can be concluded from Table 2 that the hydration number of divalent ions in the two positions is almost the same. As stated by the previous study (Bo et al. 2017), divalent ions like magnesium and calcium ions are surrounded by two shells of water molecules so that the first layer is more stable. It leads to the fact that the number of water molecules in the first hydration shell is almost constant when the ion passes through the pore, as can be inferred from Table 2. On the other hand, water molecules in the second layer can be easily separated, which requires less energy in calcium ions than in magnesium ions, and consequently, the percentage of calcium rejection is lower than that of magnesium.

3.2 Effect of the Applied Pressure

Simulations were conducted for 9 and 13 Å pore diameters to conduct a careful investigation of the influences of the applied pressure, and the number of water molecules passing through 9 and 13 Å pore at different pressures of 100, 150, and 200 MPa is represented

Table 2 Hydration number of ions in the bulk region and at a distance of 1 Å from the 9 Å nanopore

RDF region	Ion				
	Na^+	K^+	Mg^{2+}	Ca^{2+}	Cl^-
Bulk region	5.96	7.02	3.05	4.01	6.83
At a distance of 1 Å from the 9 Å pore	5.25	6.58	3.01	4.00	6.24

Fig. 10 Number of filtered water across the pristine graphene membrane with a pore diameter of 9 Å pore at different pressures of 100, 150, and 200 MPa for the left piston
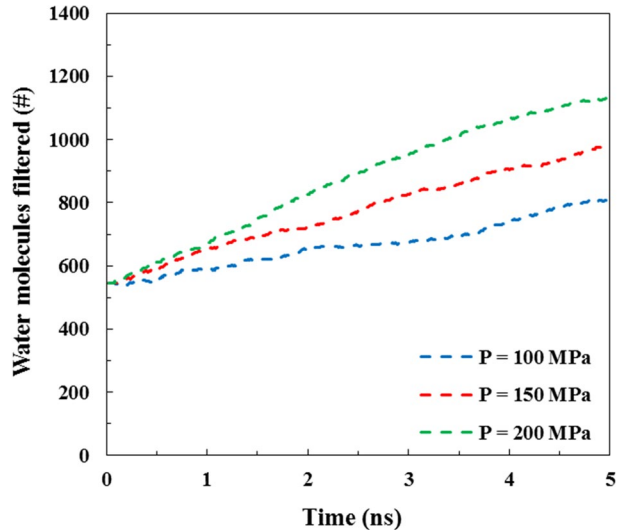
Fig. 11 Number of water molecules filtered through the pristine graphene membrane with 13 Å pore diameter at different pressures of 100, 150, and 200 MPa
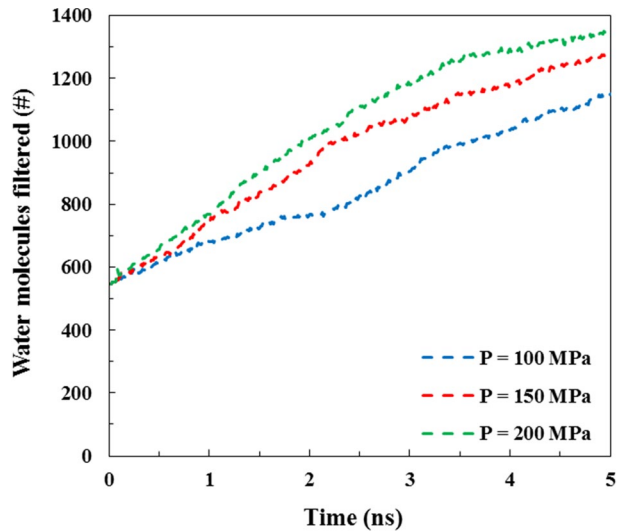
in Figs. 10 and 11, respectively. Examination of these figures reveals that in the case of 9 Å, by raising the pressure from 100 to 150 MPa, the number of filtered water molecules permeating through the membrane increases by 61%, and if the pressure reaches 200 MPa, this increment will be about 118%. Moreover, if the diameter increases to 13 Å, former values will be 21% and 34%, respectively. Hence, the effects of rising the external pressure on filtration will be greater in membranes with smaller pores. Although it is expected that in pores with larger diameters, pressure increment yields more water molecules to transport through the membrane, it should be mentioned that the accumulation of water molecules on the other side of the membrane acts as a deterrent factor for new molecules which will be more effective by increasing the diameter.

Table 3 Ions rejection for different pore diameters of 9, 11, 13, and 15 Å at the pressure of 100 and 200 MPa. The values were computed by averaging over three individual simulations

Pore diameter (Å)	Pressure (MPa)	Ion rejection (%)				
		Na^+	K^+	Mg^{2+}	Ca^{2+}	Cl^-
9	100	100	100	100	100	100
	200	100	100	100	100	100
11	100	100	100	100	100	100
	200	100	83.3	100	100	100
13	100	100	100	100	100	100
	200	100	83.3	100	100	94.4
15	100	100	66.7	100	100	97.2
	200	66.7	50	100	83.3	63.9

Table 4 Ions rejection decrement by doubling the pressure in different pore diameters of 9, 11, 13, and 15 Å

Pore diameter (Å)	Rejection decrement by doubling the pressure (%)				
	Na^+	K^+	Mg^{2+}	Ca^{2+}	Cl^-
9	0	0	0	0	0
11	0	16.7	0	0	0
13	0	16.7	0	0	5.6
15	33.3	16.7	0	16.7	33.3

Ions rejection for the pressure of 100 and 200 MPa for various pore diameters is listed in Table 3 by comparing Figs. 7 and 8. According to this table, as expected, by doubling the exerted pressure, more ions pass through the membrane. Also, Table 4 lists the rejection decrement of various ions in two pressures for different pore diameters. Examination of this table reveals that no ion passes through the membrane with the 9 Å pore by doubling the pressure. As evident from the table, this pore has 100% rejection in low and high pressures, and pressure increment does not affect its rejection performance. Therefore, this diameter can be considered an optimum pore size to have the highest rejection, even at high pressures. It indicates that the pressure increase, similar to the effect of pore diameter, has an opposite influence on water flow rate and ion rejection in such a way that it improves the permeation rate of water molecules but adversely affects ion rejection. Additionally, based on the results of the previous section, if the pore diameter is increased from 9 to 15 Å at a constant pressure of 100 MPa, the water flow rate is improved by 168%, while the performance of the membrane in rejecting potassium and chloride ions is weakened. On the other hand, the obtained results from Fig. 10 and Table 4 demonstrate that raising the pressure from 100 to 200 MPa, in the condition that the pore diameter is fixed at 9 Å, leads to a 118% improvement in water flow rate while maintaining the ion rejection at 100%. Thus, it can be claimed that doubling the pressure is a more reasonable choice to enhance the performance of the graphene membrane with a 9 Å pore diameter compared to increasing the pore diameter to 15 Å. The other considerable result of Table 4 is that rejection decrement will be higher for ions with lower hydration energy. Indeed, by increasing the exerted pressure at each pore diameter, smaller hydrated ions such as potassium and chloride have more chance to go through the membrane pore. This behavior continues until the pore diameter changes to 13 Å. As the pore diameter increases and pressure reaches 200 MPa, the pattern changes slightly, and the ions with a larger hydrated radius (sodium)

Table 5 Equilibrium bond lengths (Konatham et al. 2013) and the effective diameters of nanopore with the functional groups

FGs	Bond type	Equilibrium bond length (Å)	Effective diameter (Å)
COO⁻			
	C (GS)–C (FG)	1.41	10
	C (FG)–O (C=O)	1.22	
	C (FG)–O (C–O⁻)	1.25	
OH			
	C (GS)–O	1.36	10.7
	O–H	0.96	

Table 6 Number of water molecules passed through the unit effective surface area of the hydroxylated, carboxylated, and pristine nanopores with a diameter of 15 Å at different times. The values were computed by averaging over three individual simulations

Time (ns)	The number of water molecules passed through the unit effective surface area of the nanopore $(1/\text{Å}^2)$		
	Pristine	Carboxyl	Hydroxyl
3	5.55	8.22	9.58
5	6.01	9.66	11.21
7	6.11	10.47	11.93

may permeate through the membrane more than those with a lower hydrated radius (potassium). Although, in this situation, the ions with the highest hydration energy (i.e., magnesium) have no chance to go to the other side of the membrane, the pattern has little difference compared to the smaller diameters.

3.3 Effect of the Functional Groups

As mentioned earlier, there are two functional groups, i.e., hydroxyl and carboxyl (Fig. 3), placed in nanopores, and their effects on the water passage and ion rejection have been studied. Since a functional group reduces the nanopore diameter and affects the amount of water passing through the membrane, the effective diameter and the corresponding effective pore area should be considered. As a reasonable assumption, the effective pore diameter can be achieved by subtracting the equilibrium stretching length of a functional group from the initial nanopore diameter (Konatham et al. 2013). Also, the effective pore area can be estimated roughly using the formula $\frac{\pi}{4}d_{\text{eff}}^2$. Table 5 lists the equilibrium bond lengths of functional groups considered in the present study. In order to facilitate the comparison, the initial diameter was considered equal to 15 Å in all cases of this section. Since the effect of applied pressure on the system was studied in detail in the previous section, this variable was kept constant here. Thus, all simulations have been performed with the applied pressure of 200 MPa.

Table 6 shows the number of water molecules passed across the unit effective surface area of the nanopores at different times. According to the results, the hydroxyl groups have the highest permeability of water molecules. The reason may lie in the creation of hydrogen bonds. The hydroxyl groups with the hydrogen atom attached to the oxygen tend to

create hydrogen bonds with the water molecules. Also, a polar nanopore with carboxyl groups attracts more water molecules than a pristine nonpolar pore, which is why the carboxylated pore has a higher water flux than the pristine pore.

Moreover, Fig. 12 depicts ion rejection in the presence of different functional groups at nanoporous graphene membranes. Accordingly, the nanopore with the carboxyl groups has the highest ion rejection, and the pristine nanopore has the lowest ion removal. Furthermore, all the ions are rejected with the carboxyl groups in the nanopore. Also, it seems that the lower hydration energy of potassium ions has allowed them to pass through the hydroxylated nanopore. It should be noted that although functional groups cause the reduction in the radius of the nanopore, and it has an important effect on the ion repulsion, according to the results, reducing the radius is not the only determining factor in the possibility of passing ions. As mentioned, although the effective radius of the nanopore with the carboxyl group is approximately equal to the hydroxylated nanopore, the average ion rejection by the former is higher than the other due to the different interactions of the functional groups with the ions. Another remarkable result is that by adding hydroxyl or carboxyl groups to the nanopore, unlike increasing the pressure or pore diameter, the water transport through the membrane and the ion rejection improves simultaneously. This observation demonstrates that the application of hydroxyl or carboxyl groups is a superior choice compared to increasing the pore size or external pressure to enrich the performance of graphene.

3.4 Effect of the Contaminant Concentration

Three concentrations of 0.1, 0.2, and 0.3 mol/L were considered to investigate the influences of ion concentration on the membrane function. Figure 13 shows the number of filtered water molecules passed the graphene with a 15 Å pore diameter for different ion concentrations at the pressure of 100 MPa. Accordingly, the number of filtered water through the membrane decreases by increasing the concentration of pollutants. This observation

Fig. 12 Ion rejection of the pristine pore with a diameter of 15 Å (blue column bar), hydroxylated pore (green column bar), and carboxylated pore (red column bar) for the applied pressure of 200 MPa. The values were computed by averaging over three individual simulations
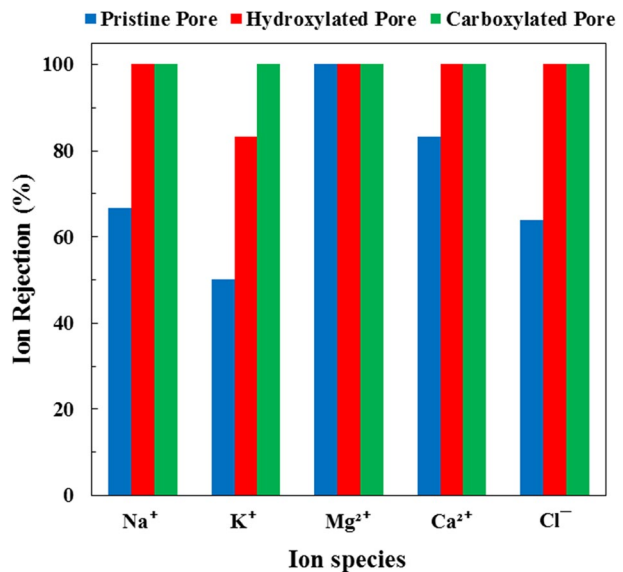
Fig. 13 Number of water molecules filtered through the 15 Å pore at the 100 MPa pressure for different ion concentrations of 0.1, 0.2, and 0.3 mol/L
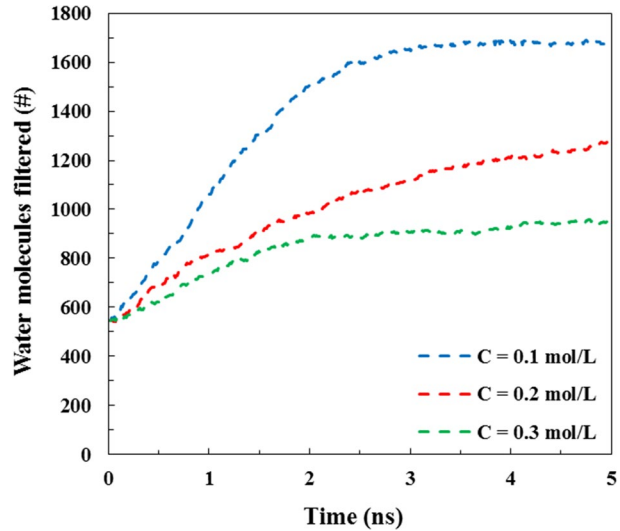
can have two reasons. The electrostatic force between the ions and the water molecules at higher concentrations causes more interaction. At the same time, water molecules are more likely to be absorbed or repelled by pollutant ions rather than they tend to cross the membrane. On the other hand, high concentrations of ions increase the possibility of nanopore obstruction and thus disrupt the passage of water from the nanoporous graphene membrane. Also, Fig. 13 shows that the curve of filtered water molecules for the concentration of 0.1 mol/L becomes horizontal after about three nanoseconds. This observation reveals the complete evacuation of water molecules on the left side of the graphene. In addition, as the concentration of the feed reservoir increases with time, the osmotic pressure within the system increases, leading to a decrease in the slope of the graphs, which is most evident for the concentration of 0.3 mol/L.

Table 7 depicts the rejection of contaminant ions at the applied pressure of 100 MPa and various concentrations for the graphene with a 15 Å pore diameter. Based on the results and as previously mentioned, ions with lower hydration energy have more chances to go through the membrane at each concentration. The results in Table 7 reveal that in all cases, the rejection percentage of potassium is less than or at least equal to sodium. It is also true in the case of calcium and magnesium, where calcium ions' rejection rate in all cases is less or at least equal to magnesium. These observations can be justified by hydration energies and hydrated radius of different ions, which were already discussed in the previous section.

Table 7 Ions rejection for various contaminant concentrations at the 100 MPa pressure and pore diameter of 15 Å. The values were computed by averaging over three individual simulations

Contaminant concentration (mol/L)	Ion rejection (%)				
	Na^+	K^+	Mg^{2+}	Ca^{2+}	Cl^-
0.1	100	100	100	100	94.4
0.2	100	67.7	100	100	97.2
0.3	88.9	77.8	100	100	92.6

4 Conclusions

Herein, the MD simulations were used to study water purification across a monolayer graphene membrane. Various contaminant ions were considered, including Na^+, K^+, Mg^{2+}, Ca^{2+}, and Cl^-. The effects of nanopores diameter, the pressure applied to the system, the contaminant concentrations, and functional groups grafted to the nanopore on water molecules filtering and ion rejection were examined, and the following results were obtained:

- As expected, more water passes through the membrane by increasing the pore diameter. Based on the results, after 5 nanoseconds and at the pressure of 100 MPa, by increasing the pore diameter from 9 to 15 Å, the number of filtered water rises by 168%.
- The hydration energy of ions has an essential effect on ion rejection. Ions with smaller hydration energy have more permeation through the single-layer graphene membrane. Also, the optimum pore diameter of 9 Å was obtained. Below this diameter, no ion can pass through the membrane, and the ion rejection is 100% for all the pollutant ions examined in this study. As the pore diameter becomes larger than 9 Å, ions begin to transmit through the membrane.
- In the case of water permeability, the effect of increasing pressure on smaller diameters is more than the larger ones. This result is important in the design of membranes, and if increasing pressure is desired, membranes with smaller diameters should be considered to reach higher efficiency.
- Although the ion rejection is expected to diminish with increasing pressure, for the nanopore with a diameter of 9 Å, by doubling the pressure from 100 to 200 MPa, in addition to improving the water flow rate by 118%, all ion species are entirely blocked by the membrane.
- Functional groups may play an essential role in the process. Among the functional groups, hydroxyl groups have the largest water permeability, and nanopores with carboxyl groups have the best rejection for different contaminant ions. Also, pore functionalization with hydroxyl or carboxyl groups, as opposed to increasing pore size or pressure, concurrently enhances water flux and ion rejection.
- In a specified pore diameter, with increasing contaminant ion concentration, the filtered water through the membrane and ion rejection decrease. It indicates that the change in concentration has similar effects on water flux and ion repulsion, contrary to the influences of pore size and pressure.

Finally, the above results can be considered in membrane design and separation of contaminant ions from water to increase the efficiency and reliability of these processes.

Data Availability The datasets generated during and/or analyzed during the current study are available from the corresponding author upon reasonable request.

Declarations

Conflict of interest On behalf of all authors, the corresponding author states that there is no conflict of interest.

References

Azamat, J., Khataee, A., Joo, S.W.: Functionalized graphene as a nanostructured membrane for removal of copper and mercury from aqueous solution: a molecular dynamics simulation study. J. Mol. Graph. Model. **53**, 112–117 (2014)

Azamat, J., Khataee, A., Joo, S.W.: Molecular dynamics simulation of trihalomethanes separation from water by functionalized nanoporous graphene under induced pressure. Chem. Eng. Sci. **127**, 285–292 (2015)

Bae, S., Kim, H., Lee, Y., Xu, X., Park, J.-S., Yi, Z., Balakrishnan, J., Lei, T., Kim, H.R., Song, Y.I., Kim, Y.-J., Kim, K.S., Özyilmaz, B., Ahn, J.-H., Hong, B.H., Iijima, S.: Roll-to-roll production of 30-inch graphene films for transparent electrodes. Nat. Nanotechnol. **5**, 574–578 (2010)

Bo, C., Haifeng, J., Xiang, L., Xuejiao, H.: Molecular insight of water desalination across multilayer graphene oxide membranes. ACS Appl. Mater. Interfaces **9**(27), 22826–22836 (2017)

Bounds, D.: A molecular dynamics study of the structure of water around the ions Li+, Na+, K+, Ca++, Ni++ and Cl-. Mol. Phys. **54**(6), 1335–1355 (1985)

Campione, A., Cipollina, A., Toet, E., Gurreri, L., Bogle, I.D.L., Micale, G.: Water desalination by capacitive electrodialysis: experiments and modelling. Desalination **473**, 114150 (2020)

Cao, H., Yu, Q., Colby, R., Pandey, D., Park, C.S., Lian, J., Zemlyanov, D., Childres, I., Drachev, V., Stach, E.A., Hussain, M., Li, H., Pei, S.S., Chen, Y.P.: Large-scale graphitic thin films synthesized on Ni and transferred to insulators: Structural and electronic properties. J. Appl. Phys. **107**(4), 044310 (2010)

Chen, S., Liu, W., Li, S.: Effect of long-range electrostatic repulsion on pore clogging during microfiltration. Phys. Rev. E **94**, 063108 (2016)

Chen, E., Jia, L., Chen, C., Huang, F., Zhang, L.: Understanding the transport mechanism of seawater through FMOF-1 and its derivative via molecular dynamics simulation. J. Mol. Liq. **325**, 115209 (2021)

Chen, Q., Yang, X.: Pyridinic nitrogen doped nanoporous graphene as desalination membrane: molecular simulation study. J. Membr. Sci. **496**, 108–117 (2015)

Chogani, A., Moosavi, A., Bagher Sarvestani, A., Shariat, M.: The effect of chemical functional groups and salt concentration on performance of single-layer graphene membrane in water desalination process: a molecular dynamics simulation study. J. Mol. Liq. **301**, 112–478 (2020)

Cohen-Tanugi, D., Grossman, J.C.: Water desalination across nanoporous graphene. Nano Lett. **12**(7), 3602–3608 (2012)

Cohen-Tanugi, D., Grossman, J.C.: Water permeability of nanoporous graphene at realistic pressures for reverse osmosis. J. Chem. Phys. **141**(7), 074704 (2014)

Cotton, F.A., Wilkinson, G., Murillo, C.A., Boch, M.: Advanced Inorganic Chemistry. Wiley, Chichester (1999)

Dang, L.X.: Mechanism and thermodynamics of ion selectivity in aqueous solutions of 18-Crown-6 Ether: a molecular dynamics study. J. Am. Chem. SOC. **26**(117), 6954–6960 (1995)

Degrève, L., Vechi, S.M., Junior, C.Q.: The hydration structure of the Na+ and K+ ions and the selectivity of their ionic channels. Biochimica Et Biophysica Acta (BBA) - Bioenergetics **1274**(3), 149–156 (1996)

Dove, P.M., Nix, C.J.: The influence of the alkaline earth cations, magnesium, calcium, and barium on the dissolution kinetics of quartz. Geochim. Cosmochim. Acta **61**(16), 3329–3340 (1997)

Kumari, P., Alam, M., Siddiqi, W.A.: Usage of nanoparticles as adsorbents for waste water treatment: an emerging trend. Sustain. Mater. Technol. **22**, e00128 (2019)

Gao, C., Zhang, M., Jiang, Z., Liao, J., Xie, X., Huang, T., Zhao, J., Bai, J., Pan, F.: Preparation of a highly water-selective membrane for dehydration of acetone by incorporating potassium montmorillonite to construct ionized water channel. Chem. Eng. Sci. **135**, 461–471 (2015)

Geim, A., Novoselov, K.: The rise of graphene. Nat. Mater. **6**, 183–191 (2007)

Havel, J., Högfeldt, E.: Evaluation of water sorption equilibrium data on Dowex ion exchanger using WSLET-MINUIT program. Scr. Fac. Sci. Nat. Univ. Masaryk. Brun. Chem. **25**, 73–84 (1995)

Heerema, S.J., Dekker, C.: Graphene nanodevices for DNA sequencing. Nat. Nanotech **11**, 127–136 (2016)

Hockney, R.W., Eastwood, J.W.: Computer Simulation Using Particles. CRC Press, Boca Raton (1988)

Hou, D., Qiao, G., Wang, P.: Molecular dynamics study on water and ions transport mechanism in nanometer channel of 13X zeolite. Chem. Eng. J. **420**, 129975 (2021)

Huang, L., Zhang, M., Li, C., Shi, G.: Graphene-based membranes for molecular separation. J. Phys. Chem. Lett. **6**(14), 2806–2815 (2015)

Impey, R.W., Madden, P.A., McDonald, I.R.: Hydration and mobility of ions in solution. J. Phys. Chem. **87**(25), 5071–5083 (1983)

Jorgensen, W.L., Chandrasekhar, J., Madura, J.D.: Comparison of simple potential functions for simulating liquid water. J. Chem. Phys. **79**(2), 926 (1983)

Jorgensen, W.L., Maxwell, D.S., Tirado-Rives, J.: Development and testing of the OPLS All-atom force field on conformational energetics and properties of organic liquids. J. Am. Chem. Soc. **45**(118), 11225–11236 (1996)

Joung, I.S., Cheatham, T.E.: Determination of Alkali and Halide monovalent ion parameters for use in explicitly solvated biomolecular simulations. J. Phys. Chem. B **112**(30), 9020–9041 (2008)

Jun, S., Tashi, T., Park, H.S.: Size dependence of the nonlinear elastic softening of nanoscale graphene monolayers under plane-strain bulge tests: a molecular dynamics study. J. Nanomater. **2011**, 380286 (2011)

Kamal Kandezi, M., Shadman Lakmehsari, M., Matta, C.F.: Electric field assisted desalination of water using B- and N-doped-graphene sheets: a non-equilibrium molecular dynamics study. J. Mol. Liq. **302**, 112574 (2020)

Kim, K.S., Zhao, Y., Jang, H., Lee, S.Y., Kim, K.S., Ahn, J.-H., Kim, P., Choi, J.-Y., Hong, B.H.: Large-scale pattern growth of graphene films for stretchable transparent electrodes. Nature **457**, 706–710 (2009)

Köhler, M. H., Bordin, J. R., Barbosa, M. C.: 2D nanoporous membrane for cation removal from water: effects of ionic valence, membrane hydrophobicity, and pore size. J. Chem. Phys. 148(22) (2018)

Konatham, D., Yu, J., Ho, T.A., Striolo, A.: Simulation insights for graphene-based water desalination membranes. Langmuir **29**(38), 11884–11897 (2013)

Kong, C.L.: Combining rules for intermolecular potential parameters. II. Rules for the Lennard-Jones (12–6) potential and the Morse potential. J. Chem. Phys. **59**(5), 2464–2467 (1973)

Lee, S.H., Rasaiah, J.C.: Molecular dynamics simulation of ion mobility. 2. Alkali metal and halide ions using the SPC/E model for water at 25 °C. J. Phys. Chem. **100**, 1420–1425 (1996)

Liu, H., Jameson, C.J., Murad, S.: Molecular dynamics simulation of ion selectivity process in nanopores. Mol. Simul. **34**(2), 169–175 (2008)

Liu, B., Wu, R., Baimova, J.A., Wu, H., Law, A.W.-K., Dmitriev, S.V., Zhou, K.: Molecular dynamics study of pressure-driven water transport through graphene bilayers. Phys. Chem. Chem. Phys. **18**(3), 1886–1896 (2016)

Liu, Y., Xie, D., Song, M., Jiang, L., Fu, G., Liu, L., Li, J.: Water desalination across multilayer graphitic carbon nitride membrane: Insights from non-equilibrium molecular dynamics simulations. Carbon **140**, 131–138 (2018b)

Liu, Y., Chen, X.: Mechanical properties of nanoporous graphene membrane. J. Appl. Phys. **115**, 034303-034303–8 (2014)

Liu, B., Law, A.W.-K., Zhou, K.: Strained single-layer C2N membrane for efficient seawater desalination via forward osmosis: a molecular dynamics study. J. Membr. Sci. **550**, 554–562 (2018a)

Loh, G.C.: Fast water desalination by carbon-doped boron nitride monolayer: transport assisted by water clustering at pores. Nanotechnology **30**(5), 055401 (2019)

Lv, F., Fang, C., Su, J.: Enhanced water transport through a carbon nanotube controlled by the lateral pressure. Nanotechnology **30**(24), 245707 (2019)

Madima, N., Mishra, S.B., Inamuddin, I., Mish, A.K.: Carbon-based nanomaterials for remediation of organic and inorganic pollutants from wastewater. A review. Environ. Chem. Lett. **18**, 1169–1191 (2020)

Marañón Di Leo, J., Marañón, J.: Confined ions and water in nanotube. J. Mol. Struct. (thoechem.) **709**(1–3), 163–166 (2004)

Meidani, K., Cao, Z., BaratiFarimani, A.: Titanium carbide MXene for water desalination: a molecular dynamics study. ACS Appl. Nano Mater. **4**(6), 6145–6151 (2021)

Mortazavi, V., Moosavi, A., Nouri-Borujerdi, A.: Enhancing water desalination in graphene-based membranes via an oscillating electric field. Desalination **495**, 114672 (2020)

Mudhoo, A., Sillanpää, M.: Magnetic nanoadsorbents for micropollutant removal in real water treatment: a review. Environ. Chem. Lett. **19**(6), 4393–4413 (2021)

Nguyen, C. T., Beskok, A.: Water desalination performance of h-BN and optimized charged graphene membranes. Microfluid Nanofluid, 24(5), (2020)

Nguyen, C.T., Beskok, A.: Charged nanoporous graphene membranes for water desalination. Phys. Chem. Chem. Phys. **21**, 9483–9494 (2019)

O'Hern, S.C., Boutilier, M.S.H., Idrobo, J.-C., Song, Y., Kong, J., Laoui, T., Atieh, M., Karnik, R.: Selective ionic transport through tunable subnanometer pores in single-layer graphene membranes. Nano Lett. **14**(3), 1234–1241 (2014)

Plimpton, S.: Fast parallel algorithms for short-range molecular dynamics. J. Comput. Phys. **117**(1), 1–19 (1995)

Qin, Q., Liu, X., Wang, H., Sun, T., Chu, F., Xie, L., Brault, P., Peng, Q.: Highly efficient desalination performance of carbon honeycomb based reverse osmosis membranes unveiled by molecular dynamics simulations. Nanotechnology **32**, 375705 (2021)

Qureshi, K., Ahmad, M.Z., Bhatti, I.A., Zahid, M., Nisar, J., Iqbal, M.: Graphene oxide decorated ZnWO4 architecture synthesis, characterization and photocatalytic activity evaluation. J. Mol. Liq. **285**, 778–789 (2019)

Reina, A., Jia, X., Ho, J., Nezich, D., Son, H., Bulovic, V., Dresselhaus, M.S., Kong, J.: Large area, few-layer graphene films on arbitrary substrates by chemical vapor deposition. Nano Lett. **9**(1), 30–35 (2009)

Rikhtehgaran, S., Lohrasebi, A.: Water desalination by a designed nanofilter of graphene-charged carbon nanotube: a molecular dynamics study. Desalination **365**, 176–181 (2015)

Robertson, A.W., Lee, G.-D., He, K., Gong, C., Chen, Q., Yoon, E., Kirkland, A.I., Warner, J.H.: Atomic structure of graphene subnanometer pores. ACS Nano **9**(12), 11599–11607 (2015)

Russo, P., Hu, A., Compagnini, G.: Synthesis, properties and potential applications of porous graphene: a review. Nano-Micro Lett. **5**(4), 260–273 (2013)

Sint, K., Wang, B., Král, P.: Selective ion passage through functionalized graphene nanopores. J. Am. Chem. Soc. **130**(49), 16448–16449 (2008)

Suk, M.E., Aluru, N.R.: Water transport through ultrathin graphene. J. Phys. Chem. Lett. **1**(10), 1590–1594 (2010)

Tansel, B.: Significance of thermodynamic and physical characteristics on permeation of ions during membrane separation: Hydrated radius, hydration free energy and viscous effects. Sep. Purif. Technol. **86**, 119–126 (2012)

Tansel, B., Sager, J., Rector, T., Garland, J., Strayer, R.F., Levine, L., Roberts, M., Hummerick, M., Bauer, J.: Significance of hydrated radius and hydration shells on ionic permeability during nanofiltration in dead end and cross flow modes. Sep. Purif. Technol. **51**(1), 40–47 (2006)

Tansel, B., Sager, J., Garland, J., Xu, S.: Effect of transmembrane pressure on overall membrane resistance during cross-flow filtration of solutions with high-ionic content. J. Memb. Sci. **325**(1–2), 205–210 (2009)

Teow, Y.H., Mohammad, A.W.: New generation nanomaterials for water desalination: a review. Desalination **451**, 2–17 (2019)

Wang, S., Sun, H., Ang, H., Tadé, M.: Adsorptive remediation of environmental pollutants using novel graphene-based nanomaterials. Chem. Eng. J. **226**, 336–347 (2013)

Wang, Y., He, Z., Gupta, K.M., Shi, Q., Lu, R.: Molecular dynamics study on water desalination through functionalized nanoporous graphene. Carbon **116**, 120–127 (2017)

Wells, A.F.: Structural inorganic chemistry. Clarendon Press, Oxford (1984)

Xue, M., Qiu, H., Guo, W.: Exceptionally fast water desalination at complete salt rejection by pristine graphyne monolayers. Nanotechnology **24**, 505720 (2013)

Yang, J., Luo, S., Zhou, X., Li, J., Fu, J., Yang, W., Wei, D.: Flexible, tunable, and ultrasensitive capacitive pressure sensor with microconformal graphene electrodes. ACS Appl. Mater. Interfaces **11**(16), 14997–15006 (2019)

Zhang, Z., Zhang, F., Liu, Z., Cheng, G., Wang, X., Ding, J.: Molecular dynamics study on the reverse osmosis using multilayer porous graphene membranes. Nanomaterials **8**(10), 805 (2018)

Zhao, W.-J., Liang, L., Kong, Z., Shen, J.-W.: A review on desalination by graphene-based biomimetic nanopore: From the computational modelling perspective. J. Mol. Liq. **342**, 117582 (2021)

Zielkiewicz, J.: Structural properties of water: comparison of the SPC, SPCE, TIP4P, and TIP5P models of water. J. Chem. Phys. **123**(10), 104501 (2005)